

# Hector V3.2.0: functionality and performance of a reduced-complexity climate model

Kalyn Dorheim<sup>1</sup>, Skylar Gering<sup>2</sup>, Robert Gieseke<sup>3</sup>, Corinne Hartin<sup>4</sup>, Leeya Pressburger<sup>1</sup>, Alexey N. Shiklomanov<sup>5</sup>, Steven J. Smith<sup>1</sup>, Claudia Tebaldi<sup>1</sup>, Dawn Woodard<sup>1,6</sup>, Ben Bond-Lamberty<sup>1</sup>

1. University Joint Global Change Research Institute, Pacific Northwest National Laboratory, 5825 University Research Ct. #3500, College Park, MD 20740 USA
2. California Institute of Technology 1200 E California Blvd, Pasadena, CA 91125 USA
3. Independent Researcher, Potsdam, Germany
4. Climate Change Division, Office of Atmospheric Protection, U.S. Environmental Protection Agency, Washington, DC, USA
5. NASA Goddard Space Flight Center, 8800 Greenbelt Rd., Greenbelt, MD, 20771 USA
6. Natural Resources Defense Council, 1152 15th St NW #300, Washington, DC 20005 [USA](#)

Correspondence to: Kalyn Dorheim ([kalyn.dorheim@pnnl.gov](mailto:kalyn.dorheim@pnnl.gov))

**Abstract.** Hector is an open-source reduced complexity climate-carbon cycle model that models critical Earth system processes on a global and annual basis. Here we present an updated version of the model, Hector V3.2.0 (hereafter Hector V3) and document its new features, implementation of new science, and performance. Significant new features include permafrost thaw, a reworked energy balance submodel, and updated parameterizations throughout. Hector V3 results are in good general agreement with historical observations of atmospheric CO<sub>2</sub> concentrations and global mean surface temperature, and its future temperature projections are consistent with more complex Earth System Model output data from the Sixth Coupled Model Intercomparison Project. We show that Hector V3 is a fully open source, flexible, performant, and robust simulator of global climate changes, note its limitations, and discuss future areas of improvement and research with respect to the model's scientific, stakeholder, and educational priorities.

## 1 Introduction

Reduced complexity climate models (RCMs) fill a critical role within the diverse climate modeling landscape (Sarofim et al., 2021). With strategically simpler representations of large-scale climate processes and dynamics in contrast to coupled Earth System Models (ESMs), RCMs are computationally efficient sources of future climate projections, able to produce large ensembles of results and explore key uncertainties at a fraction of the computational cost of a single ESM run (Kawamiya et

al., 2020). For this reason, RCMs such as Hector, MAGICC, FaIR, and the other Reduced Complexity Intercomparison Project (RCMIP) participating models (Nicholls et al., 2021; Meinshausen et al., 2011; Smith et al., 2018; Nicholls et al., 2020) have been coupled with socioeconomic models (Calvin et al., 2019); used to study climate-carbon interactions and feedbacks (Woodard et al., 2021); supported the assessment of key quantities like global temperature and the carbon budget in various Intergovernmental Panel on Climate Change (IPCC) reports (Smith et al., 2021; Forster et al., 2021); and other applications.

Hector is a globally resolved carbon-climate RCM with explicit terrestrial and ocean carbon cycles as well as active surface ocean chemistry. As a stand-alone climate model, Hector has been used in a variety of other research projects (Woodard et al., 2021; Dorheim et al., 2020; Schwarber et al., 2019; Vega-Westhoff et al., 2019; Pressburger et al., 2023) and participated in the first two phases of RCMIP (Nicholls et al., 2021, 2020). In addition, since 2015, Hector has been the climate component of the Global Change Analysis Model (GCAM) (Calvin et al., 2019) and used to explore the feedback from hydrofluorocarbon emissions from future changes in heating and cooling degree days (Hartin et al., 2021) as well as how carbon dioxide (CO<sub>2</sub>) removal technologies may impact the energy-water-land system (Fuhrman et al., 2023).

Since its initial release, model development of Hector has continued in order to reflect the advances made within the climate science and open-source software research communities, and the objective of this paper is to document the latest version of the model. We provide an overview of the model before describing the major changes and upgrades that have been made since Hector V1, focusing on the default model configuration but also describing optional settings. We then compare Hector V3 results with observations and ESM output to examine model performance, and finally discuss future areas of improvement for the model in the context of its goals of accuracy, performance, and broad accessibility.

## 2 Methods

### 2.1 Model General Description

The first version of Hector (V1) was described in detail by Hartin et al. (2015). It is a self-contained object-oriented model implemented in C++ with a modular, flexible design. While Hector produces annual output, its adaptive-time solver is capable of operating at a higher frequency to help address issues with numerical instability.

In its default configuration, all Hector runs begin after “spinup” (Thornton and Rosenbloom, 2005), in which the model runs until all carbon pools are in equilibrium; this typically requires ~300 years using the default model parametrization, and typically results in changes of a few percent in the model’s major carbon pools. After the spinup phase is complete, the main Hector run begins. A Hector run can either be “free-running” or “constrained.” By default, the model is free-running, meaning that its behavior is determined by the time series of emissions and other inputs. During a *constrained* run, the model

60 is forced to match one or more user-prescribed time series. The default free-running model uses time series from 37  
61 different emission species and 3 exogenous radiative forcers (see **Supplementary Tables 1**). These emission inputs fall into  
62 two categories. The first category consists of emissions that accumulate as greenhouse gas (GHG) concentrations. The GHG  
63 concentrations for nitrous oxide (N<sub>2</sub>O), methane (CH<sub>4</sub>), and 26 halocarbons are calculated using equations that encode a  
64 simplified relationship between emissions and concentrations (**Supplementary Tables 3-5**). The GHG concentrations for  
65 ozone (O<sub>3</sub>) are calculated from interactions between nitrogen oxides (NO<sub>x</sub>), carbon monoxide (CO), and non-methane  
66 volatile organic compound (NMVOC) emissions (Equations 42-43 in **Supplementary Table 9**). The atmospheric CO<sub>2</sub>  
67 concentrations are determined in part by the anthropogenic CO<sub>2</sub> emissions (read in as an input) and by the behavior of  
68 Hector's terrestrial and ocean carbon cycle components (**Figure 1**). The second category consists of the emissions that  
69 impact Hector's radiative forcing budget: carbon monoxide (CO), black carbon (BC), organic carbon (OC), sulfur dioxide  
70 (SO<sub>2</sub>), and ammonia (NH<sub>3</sub>). These emissions are used in equations (**Supplementary Information**) that determine aerosol  
71 concentrations and thus radiative forcings. The total radiative forcing is the sum of the forcing effects of all of Hector's  
72 atmospheric greenhouse gases, aerosols, and several additional forcing inputs (volcanic forcing, albedo).

73  
74 Total radiative forcing is then used to simulate temperature change. Hector's temperature component (Vega-Westhoff et al.,  
75 2019) is an implementation of the Diffusion Ocean Energy balance CLIMate model (Kriegler, 2005; Tanaka et al., 2007).  
76 DOECLIM is a 1-D pure diffusion ocean model that calculates changes in air temperature 2 meters over ocean/land, sea  
77 surface temperature, and within the ocean mixed layer. The sea surface and land surface temperatures from DOECLIM are  
78 used by Hector's ocean and land carbon cycles to calculate the carbon fluxes at the next time step. Hector's global mean  
79 surface temperature (GMST) is the area-weighted average of these land surface and ocean surface temperatures.

Deleted: tropospheric

## 80 2.2 Changes Since V1

81 A number of significant architectural, software, and scientific developments have been implemented since the V1 release and  
82 documentation manuscript (Hartin et al., 2015). We start by documenting these software changes before discussing other  
83 changes and new features affecting Hector's carbon cycle, radiative forcing, temperature calculations, and constrained mode  
84 capabilities.

### 85 2.2.1 Software

86 Hector is an open-source community model available on GitHub (<https://github.com/jgcri/hector>). The repository includes  
87 updated project solutions and make files to support building and running Hector from the command line or development  
88 environments such as Visual Studio (<https://visualstudio.microsoft.com/>) or Xcode (<https://developer.apple.com/xcode/>).  
89 Alternatively, users can run Hector as an R (R Core Team, 2021) package, allowing for a broader range of users given R's  
90 popularity as a data analysis and simulation tool across many scientific disciplines. The R package wrapper enabled the

92 development of the Hector User Interface (Pennington and Vernon, 2021), which allows users to run and interact with  
93 Hector results in a web browser. Other changes include updated and reduced software dependencies, automated software  
94 testing, and auto-generated online documentation. Finally, a Python wrapper Pyhector (Willner et al., 2017) is maintained by  
95 community collaborators, broadening the potential users and use cases of the model. The default model remains highly  
96 performant: even without any speed optimizations at compile time, running the 550 years (1750-2300) of a standard run  
97 takes ~0.5s on a modern laptop. The model is also straightforward to parallelize for large-ensemble analyses (Pressburger et  
98 al., 2023). Ultimately, these Hector V3 software changes have led to a more robust, transparent, and accessible community  
99 model.

### 100 2.2.2 Carbon Cycle

101 Anthropogenic CO<sub>2</sub> emissions are debited from a geological pool (named “earth” in Hector; cf. **Figure 1**) pool and added to  
102 the one-pool, global atmosphere at each timestep. Hector’s active carbon cycle is split into terrestrial land and ocean  
103 submodels.

104  
105 As described in detail by Hartin et al. (2015, 2016), Hector’s ocean carbon cycle is a four-box module, consisting of two  
106 surface-level, intermediate, and deep ocean boxes (**Figure 1**). Carbon and water mass exchange occur between the four  
107 boxes respecting simplified representations of advection and thermohaline circulation, with volume transports tuned to  
108 approximate a flow of 100 Pg C from the surface high-latitude box to the deep ocean box at steady state, simulating deep  
109 water formation. Hector solves for the marine carbonate variables (DIC, pH, alkalinity) with respect to solubility in the two  
110 surface layer boxes (Zeebe and Wolf-Gladrow, 2001). The calculation of pCO<sub>2</sub> in each surface box is based on the  
111 concentration of CO<sub>2</sub> in the ocean and its solubility, in turn a function of temperature, salinity, and pressure. At steady state,  
112 the cold high-latitude surface box (> 55° N or S) acts as a sink of carbon from the atmosphere, while the warm low-latitude  
113 (≤ 55° N or S) surface box off-gases carbon back to the atmosphere. The ocean-atmosphere flux calculation follows  
114 Takahashi et al. (2009). In Hector V3, ocean carbon cycle calculations use sea surface temperature (SST) calculated by  
115 DOECLIM (see above), and the preindustrial surface and intermediate/deep ocean carbon cycle pools are initialised from the  
116 IPCC sixth assessment report (AR6) Figure 5.12 (Canadell et al., 2021) (see **Table 1**).

117  
118 Much of the basic functionality of the model’s terrestrial carbon cycle is unchanged from the original V1 release (Hartin et  
119 al., 2015). Net primary production (NPP) is partitioned into vegetation, detritus, and soil (Figure 1); litterfall moves carbon  
120 from vegetation to the soil, and temperature-dependent, first-order decay equations control the heterotrophic release of CO<sub>2</sub>  
121 back to the atmosphere from the latter two pools (Hartin et al., 2015). By default, the terrestrial carbon cycle operates as a  
122 single, global biome, but Hector can run with an arbitrary number of independent biomes, each with its own set of carbon

123 pools and parameters; a sample multi-biome parameterization is included with the model's input files, and an example of this  
124 was documented in detail by Woodard et al. (2021).

125  
126 There are also new or changed behaviors in the Hector V3 terrestrial carbon submodel. First, previously land use change  
127 (LUC) emissions were specified as a single time series that could be positive or negative, reflecting net emission or uptake,  
128 and this value was added (subtracted) to the atmosphere and subtracted (added) from the vegetation, detritus, and soil pools  
129 (Hartin et al., 2015). In V3, these are now provided in separate input time series that must be strictly positive and correspond  
130 to the gross emissions and uptake fluxes, respectively, and because of how LUC now affects NPP (see below), are assumed  
131 to include any regrowth fluxes from previous LUC. A similar change has been made to the fossil fuel/industrial emissions,  
132 which are now specified by two gross fluxes of emissions and uptake. This provides users with more flexibility to specify  
133 how the gross fluxes result in the net flux, but no behavior change otherwise. Note that the model still accepts net fluxes if  
134 that is all that is available, as is the case for the RCMIP Shared Socioeconomic Pathway (SSP) scenarios (Nicholls et al.,  
135 2020).

136  
137 Second, LUC fluxes now affect the land carbon pools in proportion to those pools' size, not via fixed allocation fractions as  
138 previously. This is a more conservative assumption than the previous user-defined allocation approach, given the large  
139 uncertainty about LUC flux magnitudes and interactive carbon-cycle effects (Yue et al., 2020; Friedlingstein et al., 2023). In  
140 addition, in a non-spatial model such as Hector, the carbon pool sizes are governed by the total amount of carbon in the  
141 system and the first-order equations linking the pools; LUC loss is only temporary until the pools re-equilibrate. The new  
142 approach is thus simpler and in most cases will have only minor effects on model results.

143  
144 Third, terrestrial NPP is now affected by LUC: the model tracks how much cumulative carbon has been lost (or gained) due  
145 to LUC, relative to preindustrial conditions, and then adjusts NPP by this fraction in addition to the pre-existing temperature  
146 and CO<sub>2</sub> adjustments to NPP described by Hartin et al. (2015). The logic behind this change is that extensive historical  
147 deforestation is known to affect photosynthesis and NPP (Ito, 2011; Malhi et al., 2004; Kaplan et al., 2012), and in previous  
148 versions of Hector deforestation did not affect the model's NPP at all. The new behavior is:

$$NPP(t) = NPP_0 \times f(C_{atm}, \beta) \times f(LUC_v) \quad (1)$$

149 where  $t$  is the current timestep;  $NPP_0$  is pre-industrial NPP; and the two  $f$  terms represent CO<sub>2</sub> fertilization (Wang et al.,  
150 2020) and the aforementioned LUC effect on NPP. This change provides a better match with known LUC effects on  
151 terrestrial biomass and production (Winkler et al., 2021; Malhi et al., 2004). More generally, it means that Hector does not  
152 regrow vegetation after LUC-driven deforestation; regrowth fluxes should be included in the LUC inputs (see above).

153

154 Fourth, Hector V3 also includes a novel implementation of permafrost thaw, a potentially significant process affecting the  
155 earth system (Hugelius et al., 2020) that releases both CO<sub>2</sub> and CH<sub>4</sub> into the atmosphere. Hector’s permafrost  
156 implementation was fully described by Woodard et al. (2021). Briefly, permafrost is treated as a separate land carbon pool  
157 that becomes available for decomposition into both CH<sub>4</sub> and CO<sub>2</sub> once thawed (Schädel et al., 2014). The thaw rate is  
158 controlled by biome-specific land surface temperature and calibrated to be consistent with both historical data and CMIP6  
159 projections (Burke et al., 2020). Woodard et al. (2021) found that the fraction of thawed permafrost carbon available for  
160 decomposition was the most influential parameter in this approach and that adding permafrost thaw to Hector resulted in  
161 0.2–0.25 °C of additional warming over the 21<sup>st</sup> century. The addition of permafrost to the V3 model produced changes in  
162 climate and permafrost carbon pools fully consistent with those reported by Woodard et al (2021).

163

164 An optional new feature in Hector V3 is the ability to track the flow of carbon as it moves between the land and ocean  
165 carbon pools and the atmosphere (as CO<sub>2</sub>). At a user-defined start-tracking date, the model tags all carbon in each of its pools  
166 as self-originating—e.g., the soil pool is deemed to be composed of 100% soil-origin carbon. As the model then runs  
167 forward, the origin tag is retained as carbon is exchanged between the models’ various pools; if 1 Pg C with origin X is  
168 incorporated into a 19 Pg C pool with origin Y, for example, at the next timestep, the 20 Pg C pool is tracked as 5% origin X,  
169 95% origin Y. At the end of a run, detailed information about the composition of each pool at each time point can be  
170 analyzed. This capability does not affect model behavior or any outputs, although it does impose a substantial performance  
171 penalty. Carbon tracking was described in detail by Pressburger et al. (2023) and is off by default.

### 172 2.2.3 Radiative Forcing

173 At each time step, after Hector’s carbon cycle solves and all GHG concentrations are computed, Hector calculates total  
174 radiative forcing as the sum of 39 forcing effects (listed in **Supplementary Table 1**), each relative to the 1750 base year.  
175 The forcing effects for volcanoes and albedo are read in as inputs, as well as a normally-unused “miscellaneous forcing”  
176 input available for experimental manipulation. The remaining 36 forcing effects for various aerosols, aerosol-cloud  
177 interactions, pollutants, and greenhouse gases are calculated internally within Hector. The forcing effects of tropospheric O<sub>3</sub>  
178 and stratospheric H<sub>2</sub>O use the same calculations as Hartin et al. (2015). For the other forcing agents, CO<sub>2</sub>, CH<sub>4</sub>, N<sub>2</sub>O, 26  
179 halocarbons, aerosol-cloud interactions, and effects of BC, OC, SO<sub>2</sub>, and NH<sub>3</sub>, Hector V3 has adopted the forcing equations  
180 from AR6 (see **Supplementary Table 5**). Of these, the forcing effect from NH<sub>3</sub> was not previously included in Hector. In  
181 addition, the aerosol-cloud interaction forcing replaces the indirect effects of SO<sub>2</sub> forcing that was previously used to  
182 approximate the SO<sub>2</sub> and cloud interactions.

183 **2.2.4 Temperature**

184 As of V2, Hector replaced a 0-D energy balance model with DOECLIM (Vega-Westhoff et al., 2019). DOECLIM uses  
185 Hector’s total radiative forcing to determine global temperature change. DOECLIM is a four-box energy balance model,  
186 meaning that it models heat transfer within the climate system represented by four idealized boxes: land (surface), air (2  
187 meters) over land, air (2 meters) over the ocean, and sea surface (ocean mixed layer). DOECLIM uses a system of  
188 differential equations to model the temperature change in the four boxes in response to radiative forcing while accounting for  
189 the proportional differences in ocean and land masses and effective heat capacity (Tanaka et al., 2007).

190  
191 In Hector V3, DOECLIM is a fully integrated component of the model, and its outputs now affect Hector’s land carbon  
192 cycle: DOECLIM’s land temperature drives heterotrophic respiration, and sea surface temperature affects ocean carbon cycle  
193 dynamics. The difference in land and ocean temperature change, or land-ocean warming ratio, is an emergent property of  
194 DOECLIM and is used by default. Two additional parameters can be used to adjust the contributions of aerosols (BC, OC,  
195 SO<sub>2</sub>, NH<sub>3</sub>, and aerosol-cloud interactions) and volcanic forcing to global temperature. By default these are set to a value of  
196 one, with the assumption being that the forcing-temperature relationship is consistent for all forcers. These scalar terms  
197 allow users to adjust the temperature sensitivity to aerosol and volcanic forcing in uncertainty analyses or when using Hector  
198 to emulate ESMs that exhibit different sensitivities to aerosol and volcanic forcings (Dorheim et al. 2020).

199 **2.2.5 Constraints**

200 Hector can run in a “constrained” mode that allows users to overwrite a specified Hector variable with a prescribed time  
201 series. Values can be prescribed for atmospheric CO<sub>2</sub> and all other GHG concentrations (effectively resulting in a  
202 concentration-forced, not emissions-forced, run). In addition, global temperature, total radiative forcing, and net biome  
203 production (effectively turning off the model’s terrestrial carbon cycle) can also be constrained. When running in the  
204 constrained mode, user-provided values seamlessly overwrite internally-calculated ones, and thus will be used by the  
205 downstream Hector components. For example, a Hector run that uses the total total radiative forcing constraint will use the  
206 user-prescribed values to calculate energy fluxes and temperature change instead of Hector’s internally calculated total ones  
207 (see **Table 2** for more examples and details).

208  
209 The ability to run in the constrained mode is a useful feature that has a number of applications. For example, Hector’s  
210 concentration constraints enable concentration-forced experiments (e.g., 1% CO<sub>2</sub> and abrupt 4 x CO<sub>2</sub> (Eyring et al., 2016) to  
211 comply with the RCMIP protocol (Nicholls et al., 2020). In addition, constraints facilitate coupling Hector with other  
212 models: the Net Biome Production (NBP) constraint can be used to pass global NBP value from a regional terrestrial carbon  
213 cycle model to Hector, and from there, Hector’s ocean carbon cycle and climate dynamics will be calculated. Finally,  
214 running Hector in constrained mode can help diagnose model behavior. For example, concentration constraints can be used

Deleted: troposphere

Deleted: troposphere

217 after a new model development leads to an unexpected increase in global temperature. Running Hector with constrained CO<sub>2</sub>  
218 concentrations or with total RF will help the developer attribute this novel behavior to changes to Hector's carbon cycle or  
219 climate dynamics.

### 220 2.2.6 Model Parameterization

221 Hector's V3 default parameterization is mostly inherited from previous versions of Hector (Hartin et al., 2015; Vega-Westhoff  
222 et al., 2019), with the exception of when robust updated estimates are available. In particular, the V3 model uses more recent  
223 estimates published for pre-industrial NPP, CO<sub>2</sub>, CH<sub>4</sub>, and N<sub>2</sub>O concentrations, as well as estimates of the pre-industrial carbon  
224 cycle to initialize its ocean carbon pools (Table 1). Initial pre-industrial sea surface temperatures used by Hector's ocean  
225 component were updated from a CMIP5 multi-model mean to a CMIP6 multi-model mean. Historical ocean surface  
226 temperature output files from 24 CMIP6 participating models (see Supplementary Table 10) were processed to compute the  
227 area-weighted mean temperature globally, at both high (> 55°) and low (≤ 55°) latitudes from 1850 to 1860 (Table 1).

228  
229 To calibrate the final model, five additional Hector parameters were fit to comparison data using a Nelder-Mead  
230 optimization routine (Nelder and Mead, 1965) in a two-part protocol. First, the natural N<sub>2</sub>O and CH<sub>4</sub> emissions, which are  
231 assumed to be constant throughout the run, were calibrated to median AR6 N<sub>2</sub>O and CH<sub>4</sub> radiative forcing (Smith et al.,  
232 2018). Second, three Hector parameters—the CO<sub>2</sub> fertilization factor  $\beta$  (unitless), heterotrophic respiration temperature  
233 sensitivity  $Q_{10}$  (unitless), and ocean heat diffusivity  $\kappa$  (cm<sup>2</sup> s<sup>-1</sup>)—were fit to historic CO<sub>2</sub> concentrations (Meinshausen et al.,  
234 2017) and GMST (Morice et al., 2021) observations from 1850 to 2021. The Meinshausen et al. (2017) records consist of  
235 data for a single year in 1750 and then a complete time series from 1850 to 2014. We chose to use CO<sub>2</sub> and GMST because  
236 they are observed data with long time series; conversely, other potential records such as ocean and land sink estimates come  
237 from either inversions or models (Friedlingstein et al., 2023). The optimization routine simultaneously minimized the  
238 average of the two variables' mean squared errors between Hector CO<sub>2</sub> concentrations and GMST and these observed data.  
239 Parameter bounds (i.e., beyond which the optimizer was not allowed) were set at  $\pm 2\sigma$ , i.e. for a normally-distributed variable  
240 ~95% of the possible distribution was used. The best fits for  $\beta$ ,  $Q_{10}$ , and  $\kappa$  (Table 1) were then set as Hector V3's default  
241 parameters. The materials and scripts used to calibrate Hector are available in the manuscript repository  
242 ([https://github.com/JGCRI/Dorheim\\_etal\\_2024\\_GMD](https://github.com/JGCRI/Dorheim_etal_2024_GMD)) to ensure the reproducibility and transparency of the calibration  
243 process.

### 244 2.3 Model runs and analysis

245 To assess model performance, we compared Hector results with both observations and ESM projections. For the historical  
246 period, we ran Hector in its default emission-driven mode, with inputs according to the RCMIP protocol (Nicholls et al.,  
247 2021, 2020) and the default parameterization described in the previous section. Hector's GMST results from 1850 to 2021

Deleted: (

Deleted: et al., 2017)



250 were compared with HadCRUT5 (Morice et al., 2021) GMST observations, while Hector's CO<sub>2</sub> concentrations in the year  
251 1750, and then from 1850 to 2014, were compared with the CMIP6 (Meinshausen et al., 2017) CO<sub>2</sub> concentrations. We used  
252 root mean squared error (RMSE) to quantify the differences between model results and the observations. An ordinary least  
253 squares linear regression was fit to Hector results and the observational data products to provide additional insights into the  
254 goodness of fit. An R<sup>2</sup> value close to one suggests a high degree of correlation between the Hector results and the  
255 observations.

256  
257 For the future period, we first compared Hector's temperature with the AR6 near-term (2021-2024), mid-term (2041-2060),  
258 and long-term (2081-2100) warming. For this, Hector was run in emissions-driven mode using the emissions from the  
259 RCMIP (Nicholls et al., 2020) protocol. Hector's near-term, mid-term, and long-term warming were computed as the 20-  
260 year averages using the model's global mean surface temperature output.

261  
262 Second, the model was run in a *constrained mode*, in which concentrations for CO<sub>2</sub>, CH<sub>4</sub>, N<sub>2</sub>O, and 26 halocarbons from  
263 RCMIP (Nicholls et al., 2020) were prescribed, and compared with CMIP6. These concentration-driven runs were consistent  
264 with the CMIP6 protocol (Eyring et al., 2016), allowing for a direct comparison of Hector's climate dynamics with that of  
265 the ESMs. For this step, output files from 15 ESMs were processed to compute area-weighted global air, land air, and sea  
266 surface temperature anomalies. The CMIP6 models were selected based on data availability for the variables and scenarios; a  
267 complete list of models is given in **Supplementary Table 11**. We used the first available ensemble member, since the  
268 internal variability between members was unlikely to affect long-term dynamics that are the focus of RCMs (Eyring et al.,  
269 2016).

### 270 **3 Results & Discussion**

271 Hector's historical CO<sub>2</sub> concentrations from an emission-driven run are compared with the Meinshausen et al. (2017) dataset  
272 in **Figure 2**. The Hector results closely follow the observed values with a RMSE of 2.14 ppm CO<sub>2</sub> and a correlation  
273 coefficient of 0.99, indicating a good agreement between Hector's output and historical carbon cycle observations. **Figure 3**  
274 compares emission-driven Hector global mean temperature with historical observations (Morice et al., 2021). The difference  
275 between Hector's results and observations is an RMSE of 0.18 °C, which is less than the 0.36 °C standard deviation of the  
276 comparison dataset. The linear fit between Hector results and observations has an adjusted R<sup>2</sup> value of 0.87 (**Figure 3**). The  
277 recent (2012-2021) decadal average global mean surface temperature for Hector was 0.75 ± 0.09 °C. The model's most  
278 notable departure from the observational record is in the late 19<sup>th</sup> and early 20<sup>th</sup> centuries (Bauer et al., 2020; Nicholls et al.,  
279 2020). The model also generally reproduces modern-day airborne fraction values (Jones et al., 2013; Pressburger et al.,  
280 2023). The model's modern (2014-2024) decadal average sea surface temperature and ocean pH are 0.78 ± 0.08 °C and 8.1  
281 ± 0.008, respectively. Hector's land sink for 2013-2022 was 1.94 ± 0.1 Pg C yr<sup>-1</sup>, which is lower than the land sink of

282  $2.9 \pm 0.9 \text{ Pg C yr}^{-1}$  reported by the Global Carbon Project (GCP, Friedlingstein et al., 2023) during the same decade.  
283 Hector's ocean sink of  $3.08 \pm 0.13 \text{ Pg C yr}^{-1}$  is consistent with the GCP ocean sink of  $2.8 \pm 0.4 \text{ Pg C yr}^{-1}$ . Ultimately, we  
284 conclude that emission-driven Hector results are in agreement with historical temperature and CO<sub>2</sub> observations except, as  
285 noted above, for the latter half of the 19<sup>th</sup> century.  
286

287 The comparison of Hector's historical results with observations is complemented by evaluating Hector's future temperature  
288 results against CMIP6 (Figure 4) and AR6 assessed warming (Canadell et al., 2021). For the future SSP1-2.6, SSP2-4.5, and  
289 SSP5-8.5 projections, Hector's temperature outputs fall squarely within the CMIP6 model spread (Figure 4). In addition,  
290 Figure 5 shows Hector's performance in two stylized experiments, 1%CO<sub>2</sub> and 4xCO<sub>2</sub> relative to CMIP6 ESMs. These are  
291 baseline experiments of the CMIP DECK protocol (Eyring et al., 2016) designed to diagnose a model's climate sensitivity,  
292 feedback strength, provide an idealized benchmark for its transient behavior (for 1%CO<sub>2</sub>); and characterize its climate  
293 sensitivity and fast-response performance (for 4xCO<sub>2</sub>). Again the model falls squarely within the CMIP6 model spread, with  
294 no suggestion of anomalous behavior. Hector's transient climate response to cumulative CO<sub>2</sub> emissions is 1.51 °C per 1000  
295 Pg C, which is cooler than the IPCC AR6 assessed best estimate of 1.65 °C per 1000 Pg C but falls within the "very likely"  
296 range of 1.0 to 2.3 °C per 1000 Pg C (Arias et al., 2021). In general, we conclude that the model exhibits climate responses  
297 consistent with AR6 (Table 3).

#### 298 4 Conclusions

299 In this manuscript, we documented the changes and new features of Hector V3. We showed that emissions-driven Hector's  
300 historical results are generally consistent with observed CO<sub>2</sub> concentrations and global mean surface temperature, with the  
301 exception of late 19<sup>th</sup> and early 20<sup>th</sup> century cooling (Bauer et al., 2020). Hector's future projections of land, ocean, and  
302 global average temperature are consistent with a CMIP6 ensemble of models. Thus, we conclude that in the context of  
303 RCMs, Hector reproduces most global-scale historical trends and ~~outputs~~ 21<sup>st</sup>-century projections consistent with Earth  
304 system models.  
305

306 This fidelity to the current climate and future CMIP6 projections means that there are many potential use cases for Hector,  
307 but it is important for users to understand the advantages (as well as disadvantages) in using it relative to other RCMs or  
308 ESMs (Nicholls et al., 2021). The freely available R package and online interface facilitate its integration into both standard  
309 analytical pipelines as well classroom settings so that students can get hands-on experience with running a climate model and  
310 interpreting results; such educational use is supported by the fact that Hector is a well-documented open-source climate  
311 model with multiple means of running the model (Hector UI, R Hector, and C++ executable). The model's fully open-source  
312 C++ core is easy to couple with other models (Calvin et al., 2019). Using the Hector R package  
313 (<https://github.com/jgcri/hector>), it is easy to generate and analyze large ensembles of Hector results which can be used to

Deleted: produces

315 explore uncertainty spaces (Nicholls et al., 2021; Pressburger et al., 2023). Finally, Hector's performance and open, flexible  
316 calibration procedure support efforts to emulate more-complex ESMs in support of novel, computationally-intensive  
317 experiments (Lu and Ricciuto, 2019; Chen et al., 2023).

318  
319 It is also important to note Hector's limitations. The model is more complex and thus harder to understand than approaches  
320 such as FAIR (Leach et al., 2021), although comparable in complexity to MAGICC (Meinshausen et al., 2011). Hector does  
321 not account for the ocean biological pump or changes in ocean stratification; whether these errors are compensating or  
322 compounding is unclear and merits future research (Jin et al., 2020). Longer-term simulations are outside of Hector's scope,  
323 as is true of most RCMs, as the model's ocean does not include the heat storage changes that strongly affect long-term global  
324 temperature dynamics (Baggenstos et al., 2019; Abraham et al., 2013). Future work should aim at understanding/rectifying  
325 the differences between Hector's terrestrial carbon sink and other sources while remaining consistent with Hector's moderate  
326 complexity and goals; it will always be important to consider trade-offs between costs (i.e., increased complexity threatening  
327 interpretability; increased predictive uncertainty from additional model parameters; computational efficiency) and benefits  
328 (increased fidelity and representativeness) (Sarofim et al., 2021).

329  
330 Finally, in addition to continued science improvements, future versions of Hector will benefit from added infrastructure  
331 capabilities. First, the current parameter-calibration routine is relatively simple and it may be worth exploring more  
332 sophisticated model-calibration procedures (Chen et al., 2023) in future versions of Hector. In addition, a turnkey ability to  
333 do probabilistic model forecasts (Fawcett et al., 2015; Ou et al., 2021), i.e. propagating parameter distributions and  
334 uncertainty (Pressburger et al., 2023) to produce probabilities of future climate change, is an important capability that a  
335 companion R package has been developed to handle (Brown et al., 2024). Leveraging this new capability for probabilistic  
336 projects will be important for future analyses using Hector to understand the changing earth and climate system.

337 **Code Availability:** Hector V3.2.0 was used to generate the Hector results analyzed and used to generate the figures included  
338 in the main text and in the supplementary information. This version of Hector is available at  
339 <https://github.com/JGCRI/hector> at the V3.2.0 release and is archived at <https://zenodo.org/records/10698028> this includes  
340 all the initialization, emission, and concentration files. All of the code and data used to calibrate Hector, perform all model  
341 runs, and produce data visualisations are available at [https://github.com/JGCRI/Dorheim\\_etal\\_2024\\_GMD](https://github.com/JGCRI/Dorheim_etal_2024_GMD) and the GMD3  
342 release associated with this iteration of the manuscript is archived at <https://zenodo.org/records/10698650>.

343 **Data Availability:** All of the calibration, comparison data, and Hector results, along with scripts used to prepare Hector runs  
344 analyzed and used to generate the figures included in the main text and in the supplementary information, are available at

345 [https://github.com/JGCRI/Dorheim\\_etal\\_2024\\_GMD](https://github.com/JGCRI/Dorheim_etal_2024_GMD) specifically release GMD3 archived at zenodo

346 <https://zenodo.org/records/10698650> is the release associated with this iteration of the manuscript.

Deleted: <https://zenodo.org/records/10698650>

347 **Author contribution:** KD, BB, SS, SK, RG, CH, LP, AS, and DW all contributed to Hector development. CT and SS  
348 helped conceptualize model experiments. KD and BB led the preparation of the original draft and all coauthors contributed  
349 to the final draft.

350 **Competing interests:** The authors declare that they have no conflict of interest.

351 **Disclaimer:** The views expressed in this article are those of the authors and do not necessarily represent the views or policies  
352 of the U.S. Department of Energy, Environmental Protection Agency, or National Aeronautics and Space Administration.

353 **Acknowledgments:** This research was supported by the U.S. Department of Energy, Office of Science, as part of research in  
354 MultiSector Dynamics, Earth and Environmental System Modeling Program. The authors would also like to acknowledge  
355 EPA Project DW-089-92459801-8 for contributing to the radiative forcing updates including in Hector v3. The authors  
356 would also like to acknowledge Robert Link and Sven Willner for their contributions to Hector and work on R Hector and  
357 Pyhector, respectively.

## 358 References

- 359 Abraham, J. P., Baringer, M., Bindoff, N. L., Boyer, T., Cheng, L. J., Church, J. A., Conroy, J. L., Domingues, C. M., Fasullo, J. T.,  
360 Gilson, J., Goni, G., Good, S. A., Gorman, J. M., Gouretski, V., Ishii, M., Johnson, G. C., Kizu, S., Lyman, J. M., Macdonald, A. M.,  
361 Minkowycz, W. J., Moffitt, S. E., Palmer, M. D., Piola, A. R., Reseghetti, F., Schuckmann, K., Trenberth, K. E., Velicogna, I., and Willis,  
362 J. K.: A review of global ocean temperature observations: Implications for ocean heat content estimates and climate change, *Rev.*  
363 *Geophys.*, 51, 450–483, 2013.
- 364 Arias, P. A., Bellouin, N., Coppola, E., Jones, R. G., Krinner, G., Marotzke, J., Naik, V., Palmer, M. D., Plattner, G.-K., Rogelj, J., Rojas,  
365 M., Sillmann, J., Storelvmo, T., Thorne, P. W., Trewin, B., Achuta Rao, K., Adhikary, B., Allan, R. P., Armour, K., Bala, G., Barimalala,  
366 R., Berger, S., Canadell, J. G., Cassou, C., Cherchi, A., Collins, W., Collins, W. D., Connors, S. L., Corti, S., Cruz, F., Dentener, F. J.,  
367 Dereczynski, C., Di Luca, A., Diongue Niang, A., Doblus-Reyes, F. J., Dosio, A., Douville, H., Engelbrecht, F., Eyring, V., Fischer, E.,  
368 Forster, P., Fox-Kemper, B., Fuglested, J. S., Fyfe, J. C., Gillett, N. P., Goldfarb, L., Gorodetskaya, I., Gutierrez, J. M., Hamdi, R.,  
369 Hawkins, E., Hewitt, H. T., Hope, P., Islam, A. S., Jones, C., Kaufman, D. S., Kopp, R. E., Kosaka, Y., Kossin, J., Krakovska, S., Lee, J.-  
370 Y., Li, J., Mauritsen, T., Maycock, T. K., Meinshausen, M., Min, S.-K., Monteiro, P. M. S., Ngo-Duc, T., Otto, F., Pinto, I., Pirani, A.,  
371 Raghavan, K., Ranasinghe, R., Ruane, A. C., Ruiz, L., Sallée, J.-B., Samset, B. H., Sathyendranath, S., Seneviratne, S. I., Sörensson, A.  
372 A., Szopa, S., Takayabu, I., Tréguier, A.-M., van den Hurk, B., Vautard, R., von Schuckmann, K., Zachle, S., Zhang, X., and Zickfeld, K.:  
373 Technical Summary, in: *Climate Change 2021: The Physical Science Basis. Contribution of Working Group I to the Sixth Assessment*  
374 *Report of the Intergovernmental Panel on Climate Change*, edited by: Masson-Delmotte, V., Zhai, P., Pirani, A., Connors, S. L., Péan, C.,  
375 Berger, S., Caud, N., Chen, Y., Goldfarb, L., Gomis, M. I., Huang, M., Leitzell, K., Lonnoy, E., Matthews, J. B. R., Maycock, T. K.,  
376 Waterfield, T., Yelekçi, O., Yu, R., and Zhou, B., Cambridge University Press, Cambridge, United Kingdom and New York, NY, USA,  
377 33–144, 2021.
- 378 Baggenstos, D., Häberli, M., Schmitt, J., Shackleton, S. A., Birner, B., Severinghaus, J. P., Kellerhals, T., and Fischer, H.: Earth's radiative  
379 imbalance from the Last Glacial Maximum to the present, *Proceedings of the National Academy of Sciences*, 116, 14881–14886, 2019.
- 380 Bauer, S. E., Tsigaridis, K., Faluvegi, G., Kelley, M., Lo, K. K., Miller, R. L., Nazarenko, L., Schmidt, G. A., and Wu, J.: Historical

382 (1850–2014) aerosol evolution and role on climate forcing using the GISS ModelE2.1 contribution to CMIP6, *J. Adv. Model. Earth Syst.*,  
383 12, <https://doi.org/10.1029/2019ms001978>, 2020.

384 Brown, J., Smith, S., Tebaldi, C., Pressburger, L., Dorheim, K., and Bond-Lamberty, B.: Matilda v1.0: An R package for probabilistic  
385 climate projections using a reduced complexity climate model, *PLOS Climate*, in press, 2024.

386 Burke, E. J., Zhang, Y., and Krinner, G.: Evaluating permafrost physics in the Coupled Model Intercomparison Project 6 (CMIP6) models  
387 and their sensitivity to climate change, *Cryosphere*, 14, 3155–3174, 2020.

388 Calvin, K., Patel, P., Clarke, L., Asrar, G., Bond-Lamberty, B., Cui, R. Y., Vittorio, A. D., Dorheim, K., Edmonds, J., Hartin, C., and  
389 Others: GCAM v5. 1: representing the linkages between energy, water, land, climate, and economic systems, *Geoscientific Model  
390 Development*, 12, 677–698, 2019.

391 Canadell, J. G., Monteiro, P. M. S., Costa, M. H., Cotrim da Cunha, L., Cox, P. M., Eliseev, A. V., Henson, S., Ishii, M., Jaccard, S.,  
392 Koven, C., Lohila, A., Patra, P. K., Piao, S., Rogelj, J., Syampungani, S., Zaehle, S., and Zickfeld, K.: Global Carbon and other  
393 Biogeochemical Cycles and Feedbacks, in: *Climate Change 2021: The Physical Science Basis. Contribution of Working Group I to the  
394 Sixth Assessment Report of the Intergovernmental Panel on Climate Change*, edited by: Masson-Delmotte, V., Zhai, P., Pirani, A.,  
395 Connors, S. L., Péan, C., Berger, S., Caud, N., Chen, Y., Goldfarb, L., Gomis, M. I., Huang, M., Leitzell, K., Lonnoy, E., Matthews, J. B.  
396 R., Maycock, T. K., Waterfield, T., Yelekçi, O., Yu, R., and Zhou, B., Cambridge University Press, Cambridge, United Kingdom and New  
397 York, NY, USA, 673–816, 2021.

398 Chen, M., Qian, Z., Boers, N., Jakeman, A. J., Kettner, A. J., Brandt, M., Kwan, M.-P., Batty, M., Li, W., Zhu, R., Luo, W., Ames, D. P.,  
399 Barton, C. M., Cuddy, S. M., Koirala, S., Zhang, F., Ratti, C., Liu, J., Zhong, T., Liu, J., Wen, Y., Yue, S., Zhu, Z., Zhang, Z., Sun, Z., Lin,  
400 J., Ma, Z., He, Y., Xu, K., Zhang, C., Lin, H., and Lü, G.: Iterative integration of deep learning in hybrid Earth surface system modelling,  
401 *Nature Reviews Earth & Environment*, 4, 568–581, 2023.

402 Dorheim, K., Link, R., Hartin, C., Kravitz, B., and Snyder, A.: Calibrating Simple Climate Models to Individual Earth System Models:  
403 Lessons Learned From Calibrating Hector, *Life Support Biosph. Sci.*, 7, e2019EA000980, 2020.

404 Eyring, V., Bony, S., Meehl, G. A., Senior, C. A., Stevens, B., Stouffer, R. J., and Taylor, K. E.: Overview of the Coupled Model  
405 Intercomparison Project Phase 6 (CMIP6) experimental design and organization, *Geosci. Model Dev.*, 9, 1937–1958, 2016.

406 Fawcett, A. A., Iyer, G. C., Clarke, L. E., Edmonds, J. A., Hultman, N. E., McJeon, H. C., Rogelj, J., Schuler, R., Alsalam, J., Asrar, G. R.,  
407 Creason, J., Jeong, M., McFarland, J., Mundra, A., and Shi, W.: CLIMATE POLICY. Can Paris pledges avert severe climate change?,  
408 *Science*, 350, 1168–1169, 2015.

409 Forster, P., Storelvmo, T., Armour, K., Collins, W., Dufresne, J.-L., Frame, D., Lunt, D. J., Mauritsen, T., Palmer, M. D., Watanabe, M.,  
410 Wild, M., and Zhang, H.: The Earth's Energy Budget, Climate Feedbacks, and Climate Sensitivity, in: *Climate Change 2021: The Physical  
411 Science Basis. Contribution of Working Group I to the Sixth Assessment Report of the Intergovernmental Panel on Climate Change*,  
412 edited by: Masson-Delmotte, V., Zhai, P., Pirani, A., Connors, S. L., Péan, C., Berger, S., Caud, N., Chen, Y., Goldfarb, L., Gomis, M. I.,  
413 Huang, M., Leitzell, K., Lonnoy, E., Matthews, J. B. R., Maycock, T. K., Waterfield, T., Yelekçi, O., Yu, R., and Zhou, B., Cambridge  
414 University Press, Cambridge, United Kingdom and New York, NY, USA, 923–1054, 2021.

415 Friedlingstein, P., Jones, M. W., Andrew, R. M., Bakker, D. C. E., Hauck, J., Landschützer, P., Le Quéré, C., Lujikx, I. T., Peters, G. P.,  
416 Peters, W., Pongratz, J., Schwingshackl, C., Sitch, S., Canadell, J. G., Ciais, P., Jackson, R. B., Alin, S. R., Anthoni, P., Barbero, L., Bates,  
417 N. R., Becker, M., Bellouin, N., Decharme, B., Bopp, L., Brasika, I. B. M., Cadule, P., Chamberlain, M. A., Chandra, N., Chau, T.-T.,  
418 Chevallier, F., Chini, L. P., Cronin, M., Dou, X., Enyo, K., Evans, W., Falk, S., Feely, R. A., Feng, L., Ford, D. J., Gasser, T., Ghattas, J.,  
419 Gkritzalis, T., Grassi, G., Gregor, L., Gruber, N., Gürses, Ö., Harris, I., Hefner, M., Heinke, J., Houghton, R. A., Hurtt, G. C., Iida, Y.,  
420 Ilyina, T., Jacobson, A. R., Jain, A., Jamiková, T., Jersild, A., Jiang, F., Jin, Z., Joos, F., Kato, E., Keeling, R. F., Kennedy, D., Klein  
421 Goldewijk, K., Knauer, J., Korsbakken, J. I., Körtzinger, A., Lan, X., Lefèvre, N., Li, H., Liu, J., Liu, Z., Ma, L., Marland, G., Mayot, N.,  
422 McGuire, P. C., McKinley, G. A., Meyer, G., Morgan, E. J., Munro, D. R., Nakaoka, S.-I., Niwa, Y., Olsen, A., Omar, A. M., Ono, T.,  
423 Paulsen, M., Pierrot, D., Pöcöck, K., Poulter, B., Powis, C. M., Rehder, G., Resplandy, L., Robertson, E., Rödenbeck, C., Rosan, T. M.,  
424 Schwinger, J., Séférian, R., Smallman, T. L., Smith, S. M., et al.: Global Carbon Budget 2023, *Earth System Science Data*, 15, 5301–5369,  
425 2023.

426 Fuhrman, J., Bergero, C., Weber, M., Monteith, S., Wang, F. M., Clarens, A. F., Doney, S. C., Shobe, W., and McJeon, H.: Diverse carbon  
427 dioxide removal approaches could reduce impacts on the energy–water–land system, *Nat. Clim. Chang.*, 13, 341–350, 2023.

428 Hartin, C., Link, R., Patel, P., Mundra, A., Horowitz, R., Dorheim, K., and Clarke, L.: Integrated modeling of human-earth system  
429 interactions: An application of GCAM-fusion, *Energy Econ.*, 103, 105566, 2021.

430 Hartin, C. A., Patel, P., Schwarber, A., Link, R. P., and Bond-Lamberty, B. P.: A simple object-oriented and open-source model for  
431 scientific and policy analyses of the global climate system – Hector v1.0, *Geoscientific Model Development*, 8, 939–955, 2015.

432 Hartin, C. A., Bond-Lamberty, B., Patel, P., and Mundra, A.: Ocean acidification over the next three centuries using a simple global  
433 climate carbon-cycle model: projections and sensitivities, *Biogeosciences*, 4329–4342, 2016.

434 Hugelius, G., Loisel, J., Chadburn, S., Jackson, R. B., Jones, M., MacDonald, G., Marushchak, M., Olefeldt, D., Packalen, M., Siewert, M.  
435 B., Treat, C., Turetsky, M., Voigt, C., and Yu, Z.: Large stocks of peatland carbon and nitrogen are vulnerable to permafrost thaw, *Proc.  
436 Natl. Acad. Sci. U. S. A.*, <https://doi.org/10.1073/pnas.1916387117>, 2020.

437 Ito, A.: A historical meta-analysis of global terrestrial net primary productivity: Are estimates converging?, *Glob. Chang. Biol.*, 17, 3161–  
438 3175, 2011.

439 Jin, D., Hoagland, P., and Buesseler, K. O.: The value of scientific research on the ocean’s biological carbon pump, *Sci. Total Environ.*,  
440 749, 141357, 2020.

441 Jones, C. D., Robertson, E., Arora, V., Friedlingstein, P., Shevliakova, E., Bopp, L., Brovkin, V., Hajima, T., Kato, E., Kawamiya, M.,  
442 Liddicoat, S., Lindsay, K., Reick, C. H., Roelandt, C., Segsneider, J., and Tjiputra, J.: Twenty-first-century compatible CO2 emissions  
443 and airborne fraction simulated by CMIP5 earth system models under four representative concentration pathways, *J. Clim.*, 26, 4398–  
444 4413, 2013.

445 Kaplan, J. O., Krumhardt, K. M., and Zimmerman, N. E.: The effects of land use and climate change on the carbon cycle of Europe over  
446 the past 500 years, *Glob. Chang. Biol.*, 18, 902–914, 2012.

447 Kawamiya, M., Hajima, T., Tachiiri, K., Watanabe, S., and Yokohata, T.: Two decades of Earth system modeling with an emphasis on  
448 Model for Interdisciplinary Research on Climate (MIROC), *Progress in Earth and Planetary Science*, 7, 1–13, 2020.

449 Kriegler, E.: *Imprecise probability analysis for integrated assessment of climate change*, Verlag nicht ermittelbar, 2005.

450 Leach, N. J., Jenkins, S., Nicholls, Z., Smith, C. J., Lynch, J., Cain, M., Walsh, T., Wu, B., Tsutsui, J., and Allen, M. R.: FaIRv2.0.0: a  
451 generalized impulse response model for climate uncertainty and future scenario exploration, *Geosci. Model Dev.*, 14, 3007–3036, 2021.

452 Lu, D. and Ricciuto, D.: Efficient surrogate modeling methods for large-scale Earth system models based on machine-learning techniques,  
453 *Geoscientific Model Development*, 12, 1791–1807, 2019.

454 Malhi, Y., Phillips, O. L., Cramer, W., Bondeau, A., Schaphoff, S., Lucht, W., Smith, B., and Sitch, S.: Tropical forests and the global  
455 carbon cycle: impacts of atmospheric carbon dioxide, climate change and rate of deforestation, *Philos. Trans. R. Soc. Lond. B Biol. Sci.*,  
456 359, 331–343, 2004.

457 Meinshausen, M., Raper, S. C. B., and Wigley, T. M. L.: Emulating coupled atmosphere-ocean and carbon cycle models with a simpler  
458 model, *MAGICC6 – Part 1: Model description and calibration*, *Atmos. Chem. Phys.*, 11, 1417–1456, 2011.

459 Meinshausen, M., Vogel, E., Nauels, A., Lorbacher, K., Meinshausen, N., Etheridge, D. M., Fraser, P. J., Montzka, S. A., Rayner, P. J.,  
460 Trudinger, C. M., Krummel, P. B., Beyerle, U., Canadell, J. G., Daniel, J. S., Enting, I. G., Law, R. M., Lunder, C. R., O’Doherty, S.,  
461 Prinn, R. G., Reimann, S., Rubino, M., Velders, G. J. M., Vollmer, M. K., Wang, R. H. J., and Weiss, R.: Historical greenhouse gas  
462 concentrations for climate modelling (CMIP6), *Geoscientific Model Development*, 10, 2057–2116, 2017.

463 Morice, C. P., Kennedy, J. J., Rayner, N. A., Winn, J. P., Hogan, E., Killick, R. E., Dunn, R. J. H., Osborn, T. J., Jones, P. D., and  
464 Simpson, I. R.: An updated assessment of near-surface temperature change from 1850: The HadCRUT5 data set, *J. Geophys. Res.*, 126,  
465 <https://doi.org/10.1029/2019jd032361>, 2021.

466 Nelder, J. A. and Mead, R.: A simplex method for function minimization, *Comput. J.*, 7, 308–313, 1965.

467 Nicholls, Z., Meinshausen, M., Lewis, J., Corradi, M. R., Dorheim, K., Gasser, T., Gieseke, R., Hope, A. P., Leach, N. J., McBride, L. A.,  
468 Quilcaille, Y., Rogelj, J., Salawitch, R. J., Samset, B. H., Sandstad, M., Shiklomanov, A., Skeie, R. B., Smith, C. J., Smith, S. J., Su, X.,

469 Tsutsui, J., Vega-Westhoff, B., and Woodard, D. L.: Reduced Complexity Model Intercomparison Project Phase 2: Synthesizing Earth  
470 System Knowledge for Probabilistic Climate Projections, *Earths Future*, 9, e2020EF001900, 2021.

471 Nicholls, Z. R. J., Meinshausen, M., Lewis, J., Gieseke, R., Dommenges, D., Dorheim, K., Fan, C.-S., Fuglested, J. S., Gasser, T.,  
472 Golik, U., Goodwin, P., Hartin, C., Hope, A. P., Kriegler, E., Leach, N. J., Marchegiani, D., McBride, L. A., Quilcaille, Y., Rogelj, J.,  
473 Salawitch, R. J., Samset, B. H., Sandstad, M., Shiklomanov, A. N., Skeie, R. B., Smith, C. J., Smith, S., Tanaka, K., Tsutsui, J., and Xie,  
474 Z.: Reduced Complexity Model Intercomparison Project Phase 1: introduction and evaluation of global-mean temperature response,  
475 *Geosci. Model Dev.*, 13, 5175–5190, 2020.

476 Nijse, F. J. M. M., Cox, P. M., and Williamson, M. S.: Emergent constraints on transient climate response (TCR) and equilibrium climate  
477 sensitivity (ECS) from historical warming in CMIP5 and CMIP6 models, *Earth Syst. Dyn.*, 11, 737–750, 2020.

478 Ou, Y., Iyer, G., Clarke, L., Edmonds, J., Fawcett, A. A., Hultman, N., McFarland, J. R., Binsted, M., Cui, R., Fyson, C., Geiges, A.,  
479 Gonzales-Zuñiga, S., Gidden, M. J., Höhne, N., Jeffery, L., Kuramochi, T., Lewis, J., Meinshausen, M., Nicholls, Z., Patel, P., Ragnauth,  
480 S., Rogelj, J., Waldhoff, S., Yu, S., and McJeon, H.: Can updated climate pledges limit warming well below 2°C?, *Science*, 374, 693–695,  
481 2021.

482 Pennington, S. and Vernon, C.: HectorUI: An Interactive Climate Model, IN33B–05, 2021.

483 Pressburger, L. and Dorheim, K. R.: JGCRI/hector\_cmip6data: v1.0, <https://doi.org/10.5281/zenodo.7304553>, 2022.

484 Pressburger, L., Dorheim, K., Keenan, T., McJeon, H., Smith, S., and Bond-Lamberty, B.: Quantifying airborne fraction trends and the  
485 destination of anthropogenic CO<sub>2</sub> by tracking carbon flows in a simple climate model, *Environ. Res. Lett.*, in press, 2023.

486 R Core Team: R: A Language and Environment for Statistical Computing v4.1.0, R Foundation for Statistical Computing, Vienna, Austria,  
487 2021.

488 Sarofim, M. C., Smith, J. B., St Juliana, A., and Hartin, C.: Improving reduced complexity model assessment and usability, *Nat. Clim.*  
489 *Chang.*, 11, 1–3, 2021.

490 Schädel, C., Schuur, E. A. G., Bracho, R., Elberling, B., Knoblauch, C., Lee, H., Luo, Y., Shaver, G. R., and Turetsky, M. R.: Circumpolar  
491 assessment of permafrost C quality and its vulnerability over time using long-term incubation data, *Glob. Chang. Biol.*, 20, 641–652, 2014.

492 Schwarber, A. K., Smith, S. J., Hartin, C. A., Vega-Westhoff, B. A., and Sriver, R.: Evaluating climate emulation: fundamental impulse  
493 testing of simple climate models, *Earth Syst. Dynam.*, 10, 729–739, 2019.

494 Smith, C., Nicholls, Z. R. J., Armour, K., Collins, W., Forster, P., Meinshausen, M., Palmer, M. D., and Watanabe, M.: The Earth’s  
495 Energy Budget, Climate Feedbacks, and Climate Sensitivity Supplementary Material, in: *Climate Change 2021: The Physical Science*  
496 *Basis. Contribution of Working Group I to the Sixth Assessment Report of the Intergovernmental Panel on Climate Change*, edited by:  
497 Masson-Delmotte, V., Zhai, P., Pirani, A., Connors, S. L., Péan, C., Berger, S., Caud, N., Chen, Y., Goldfarb, L., Gomis, M. I., Huang, M.,  
498 Leitzell, K., Lonnoy, E., Matthews, J. B. R., Maycock, T. K., Waterfield, T., Yelekçi, O., Yu, R., and Zhou, B., 2021.

499 Smith, C. J., Kramer, R. J., Myhre, G., Forster, P. M., Soden, B. J., Andrews, T., Boucher, O., Faluvegi, G., Fläschner, D., Hodnebrog, Ø.,  
500 Kasoar, M., Khari, V., Kirkevåg, A., Lamarque, J.-F., Mülmenstädt, J., Olivić, D., Richardson, T., Samset, B. H., Shindell, D., Stier, P.,  
501 Takemura, T., Voulgarakis, A., and Watson-Parris, D.: Understanding Rapid Adjustments to Diverse Forcing Agents, *Geophys. Res. Lett.*,  
502 45, 12,023–12,031, 2018.

503 Takahashi, T., Sutherland, S. C., Wanninkhof, R., Sweeney, C., Feely, R. A., Chipman, D. W., Hales, B., Friederich, G., Chavez, F.,  
504 Sabine, C., Watson, A., Bakker, D. C. E., Schuster, U., Metzl, N., Yoshikawa-Inoue, H., Ishii, M., Midorikawa, T., Nojiri, Y., Körtinger,  
505 A., Steinhoff, T., Hoppema, M., Olafsson, J., Armarson, T. S., Tilbrook, B., Johannessen, T., Olsen, A., Bellerby, R., Wong, C. S., Delille,  
506 B., Bates, N. R., and de Baar, H. J. W.: Climatological mean and decadal change in surface ocean pCO<sub>2</sub>, and net sea-air CO<sub>2</sub> flux over the  
507 global oceans, *Deep Sea Res. Part 2 Top. Stud. Oceanogr.*, 56, 554–577, 2009.

508 Tanaka, K., Kriegler, E., Bruckner, T., Hooss, G., Knorr, W., Raddatz, T. J., and Tol, R.: Aggregated carbon cycle, atmospheric chemistry,  
509 and climate model (ACC2), Institute, Max Planck, Hamburg, 188 pp., 2007.

510 Thornton, P. E. and Rosenbloom, N. A.: Ecosystem model spin-up: Estimating steady state conditions in a coupled terrestrial carbon and  
511 nitrogen cycle model, *Ecol. Modell.*, 189, 25–48, 2005.

- 512 Vega-Westhoff, B., Sriver, R. L., Hartin, C. A., Wong, T. E., and Keller, K.: Impacts of observational constraints related to sea level on  
513 estimates of climate sensitivity, *Earths Future*, 7, 677–690, 2019.
- 514 Wang, S., Zhang, Y., Ju, W., Chen, J. M., Ciais, P., Cescatti, A., Sardans, J., Janssens, I. A., Wu, M., Berry, J. A., Campbell, E.,  
515 Fernández-Martínez, M., Alkama, R., Sitch, S., Friedlingstein, P., Smith, W. K., Yuan, W., He, W., Lombardozzi, D., Kautz, M., Zhu, D.,  
516 Lienert, S., Kato, E., Poulter, B., Sanders, T. G. M., Krüger, I., Wang, R., Zeng, N., Tian, H., Vuichard, N., Jain, A. K., Wiltshire, A.,  
517 Haverd, V., Goll, D. S., and Peñuelas, J.: Recent global decline of CO<sub>2</sub> fertilization effects on vegetation photosynthesis, *Science*, 370,  
518 1295–1300, 2020.
- 519 Willner, S., Hartin, C., and Gieseke, R.: pyhector: A Python interface for the simple climate model Hector, *J. Open Source Softw.*, 2, 248,  
520 2017.
- 521 Winkler, K., Fuchs, R., Rounsevell, M., and Herold, M.: Global land use changes are four times greater than previously estimated, *Nat.*  
522 *Commun.*, 12, 2501, 2021.
- 523 Woodard, D. L., Shiklomanov, A. N., Kravitz, B., Hartin, C., and Bond-Lamberty, B.: A permafrost implementation in the simple carbon–  
524 climate model Hector v.2.3pf, *Geosci. Model Dev.*, 14, 4751–4767, 2021.
- 525 Yue, C., Ciais, P., Houghton, R. A., and Nassikas, A. A.: Contribution of land use to the interannual variability of the land carbon cycle,  
526 *Nat. Commun.*, 11, 3170, 2020.
- 527 Zeebe, R. E. and Wolf-Gladrow, D.: *CO<sub>2</sub> in Seawater: Equilibrium, Kinetics, Isotopes*, Gulf Professional Publishing, 346 pp., 2001.
- 528



529 **Table 1. Default Hector parameter values and their sources.** The parameter name column is the name as it appears in the  
 530 model's ini (initialization) files. This is not an exhaustive table of Hector parameters but rather contains the parameters that  
 531 have been updated since Hartin et al. (2015). For a complete collection of parameter values and their sources, refer to the  
 532 default initialization files available at <https://github.com/JGCRI/hector/tree/main/inst/input>. Preindustrial values here are  
 533 assumed to be circa 1745, the start of a Hector run.

Parameter	Description	Value	Units	Source
CH4N	Natural CH <sub>4</sub> Emissions are assumed to be constant over the historical and future period	338	Tg CH <sub>4</sub> yr <sup>-1</sup>	See section 2.2.6 for details
N2ON	Natural N <sub>2</sub> O emissions, assumed to be constant of the historical and future period	9.7	Tg N yr <sup>-1</sup>	
beta	CO <sub>2</sub> fertilization factor ( $\beta$ ) (increase in NPP productivity with increasing CO <sub>2</sub> concentrations)	0.55	unitless	
q10_rh	Heterotrophic respiration temperature sensitivity factor ( $Q_{10}$ )	2.2	unitless	
diff	Vertical ocean heat diffusivity ( $\kappa$ ), the rate of heat diffuses into the ocean	1.16	cm <sup>2</sup> /s	
preind_surface_c	Initial size of the preindustrial surface ocean carbon pool	900	Pg C	Figure 5.12 (Canadell et al., 2021)
preind_interdeep_c	Initial size of the preindustrial intermediate and deep ocean carbon pool	37100	Pg C	
C0	Preindustrial CO <sub>2</sub> concentration	277.15	ppmv CO <sub>2</sub>	Table 7.SM.1 (Smith et al., 2021)
N0	Preindustrial N <sub>2</sub> O concentration	273.87	ppbv N <sub>2</sub> O	
M0	Preindustrial CH <sub>4</sub> concentration	731.41	ppbv CH <sub>4</sub>	
npp_flux0	Preindustrial net primary production	56.2	Pg C yr <sup>-1</sup>	Ito (2011)
TOS0	Mean preindustrial absolute ocean air temperature	18	°C	

Deleted: /

Deleted: /

Deleted:  $\beta$

Deleted: /

538

deltaHL0	Difference between high latitude preindustrial ocean temp and TOS0	-16.4	°C	From processed CMIP6 data (Pressburger and Dorheim, 2022)
deltaLL0	Difference between low latitude preindustrial ocean temp and TOS0	2.9	°C	

539 **Table 2: Descriptions and summaries of the Hector constraints.** The constraint name column reflects the name as it  
 540 appears in the model's ini (initialization) files.

Name	Description	Implementation
CO2_constrain	Time series of CO <sub>2</sub> concentration values (ppmv CO <sub>2</sub> )	CO <sub>2</sub> radiative forcing (RF) is calculated from the user-provided CO <sub>2</sub> concentrations and then used to calculate total RF and temperature. If needed, CO <sub>2</sub> is debited/credited to/from the deep ocean to meet the CO <sub>2</sub> concentration constraint and satisfy Hector's global carbon cycle mass balance check.
CH4_constrain	Time series of CH <sub>4</sub> concentration values (ppbv CH <sub>4</sub> )	CH <sub>4</sub> RF is calculated from the user-provided CH <sub>4</sub> concentrations, feeding into total RF and temperature.
N2O_constrain	Time series of N <sub>2</sub> O concentration values (ppbv N <sub>2</sub> O)	N <sub>2</sub> O RF is calculated from the user-provided N <sub>2</sub> O concentrations.
X_constrain (X is the identifier for one of 26 halocarbons modeled by Hector)	Time series for a single halocarbon concentration (pptv)	RF for halocarbon X is calculated from the user-provided concentrations.
RF_tot_constrain	Time series of total radiative forcing value (W m <sup>-2</sup> )	User-provided total RF values are used to calculate temperature and heat flux. In this case, the emission inputs do not drive model behavior.
NBP_constrain	Time series of Net Biome Production values (Pg C yr <sup>-1</sup> )	User-provided NBP values are used to up/downscale NPP and RH so that their total matches the constraint. This effectively bypasses the model's terrestrial carbon cycle.
tas_constrain	Time series of global mean air temperature values (°C)	User-provided temperature values overwrite Hector's, with a smooth transition between the constrained and free-running behavior.

541 **Table 3. Key emergent climate metrics, historical warming, effective radiative forcing, and future warming from**  
542 **Hector versus the IPCC AR6 ‘best estimates’ from the AR6 Table 7.SM.4.** The Hector values were generated from runs  
543 using Hector's default parameterization in the free-running emission-driven mode for historical and SSP scenarios. The  
544 parenthetical IPCC AR6 values indicate the AR6 ‘very likely’ (5-95)% ranges. Acronyms include equilibrium climate  
545 sensitivity (ECS), transient climate response to cumulative carbon emissions (TCRE), transient climate response (TCR),  
546 global surface air temperature (GSAT), and effective radiative forcing (ERF) (Nijse et al., 2020).

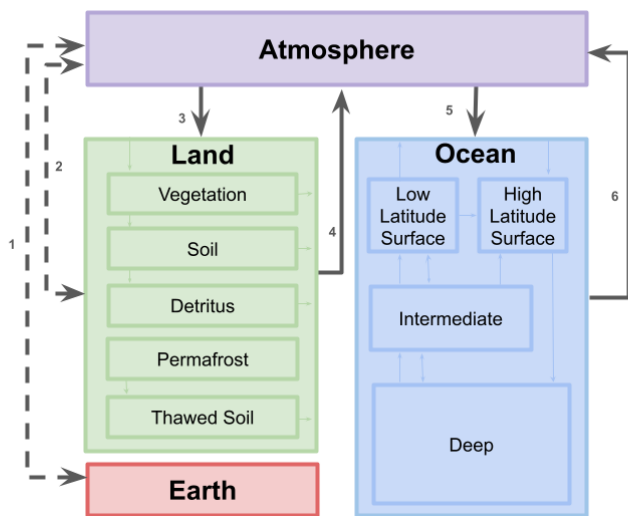
Key Metrics		Hector	IPCC AR6
ECS (°C)		3	3 (2, 5)
TCRE (°C per 1000 GtC)		1.51	1.65 (1, 2.3)
TCR (°C)		1.84	1.8 (1.2, 2.4)
Historical Warming and Effective Radiative Forcing			
GSAT Warming (°C, 1995-2014 relative to 1850-1900)		0.73	0.85 (0.67, 0.98)
Ocean heat content change (ZJ, 1971-2018)		471	396 (329, 463)
Total Aerosol ERF (W m <sup>-2</sup> , 2005-2015 relative to 1750)		-1.24	-1.3 (-2, -0.6)
WMGHG ERF (W m <sup>-2</sup> , 2019 relative to 1750)		3.87	3.32 (3.03, 3.61)
Methane ERF (W m <sup>-2</sup> , 2019 relative to 1750)		0.54	0.54 (0.43, 0.65)
Future Warming (GSAT, °C relative to 1995-2014)			
SSP1-1.19	2021-2040	0.73	0.61 (0.38, 0.85)
	2041-2060	0.90	0.71 (0.4, 1.07)
	2081-2100	0.72	0.56 (0.24, 0.96)
SSP1-2.6	2021-2040	0.75	0.63 (0.41, 0.89)

	2041-2060	1.08	0.88 (0.54, 1.32)
	2081-2100	1.10	0.90 (0.51, 1.48)
SSP2-4.5	2021-2040	0.75	0.66 (0.44, 0.90)
	2041-2060	1.29	1.12 (0.78, 1.57)
	2081-2100	1.98	1.81 (1.24, 2.59)
SSP3-7.0	2021-2040	0.76	0.67 (0.45, 0.92)
	2041-2060	1.43	1.28 (0.92, 1.75)
	2081-2100	2.94	2.76 (2.00, 3.75)
SSP5-8.5	2021-2040	0.88	0.76 (0.51, 1.04)
	2041-2060	1.74	1.54 (1.08, 2.08)
	2081-2100	3.79	3.50 (2.44, 4.82)

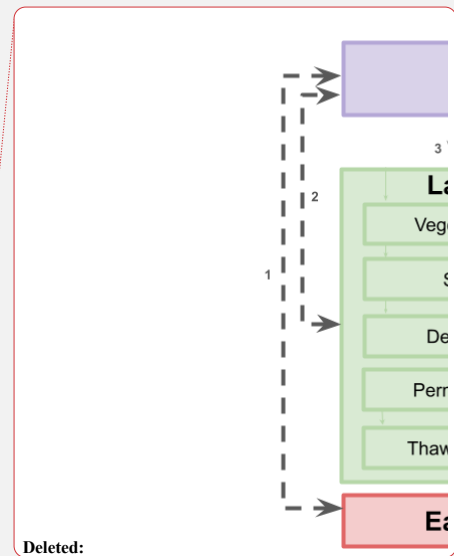
547

548

549 **Figure 1. Conceptual diagram of the CO<sub>2</sub> fluxes (numbered thick gray arrows) between Hector’s four major carbon**  
 550 **cycle boxes: a well-mixed atmosphere (Atmosphere), terrestrial carbon cycle (Land), ocean carbon cycle (Ocean), and**  
 551 **geological fossil fuel reservoir (Earth).** The thinner arrows within the land and ocean boxes allude to Hector's more  
 552 complex submodule carbon cycle dynamics, which are not discussed in detail here. The solid lines indicate that CO<sub>2</sub> fluxes  
 553 are calculated within Hector, whereas the dashed lines indicate that the fluxes are externally defined inputs read into the  
 554 model; two-headed arrows imply a potential two-way exchange of carbon. The fluxes are: (1) CO<sub>2</sub> emissions from fossil  
 555 fuels and industry and uptake of carbon capture technologies; (2) CO<sub>2</sub> emissions and uptake from land use change (e.g.,  
 556 afforestation, deforestation, etc.); (3) vegetation uptake from the atmosphere (4) the aggregate CO<sub>2</sub> from respiration from the  
 557 terrestrial biosphere; and ocean carbon (5) uptake and (6) outgassing. The model’s permafrost implementation (Woodard et  
 558 al., 2021) emits both CO<sub>2</sub> and CH<sub>4</sub> into the atmosphere from its “Thawed Soil” pool, whereas the “Soil” pool emits only  
 559 heterotrophic CO<sub>2</sub> respiration.

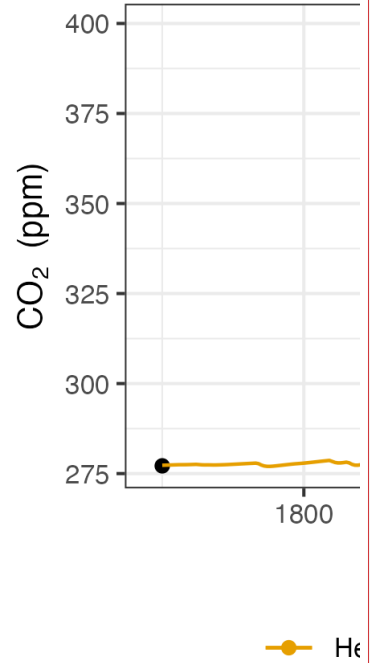
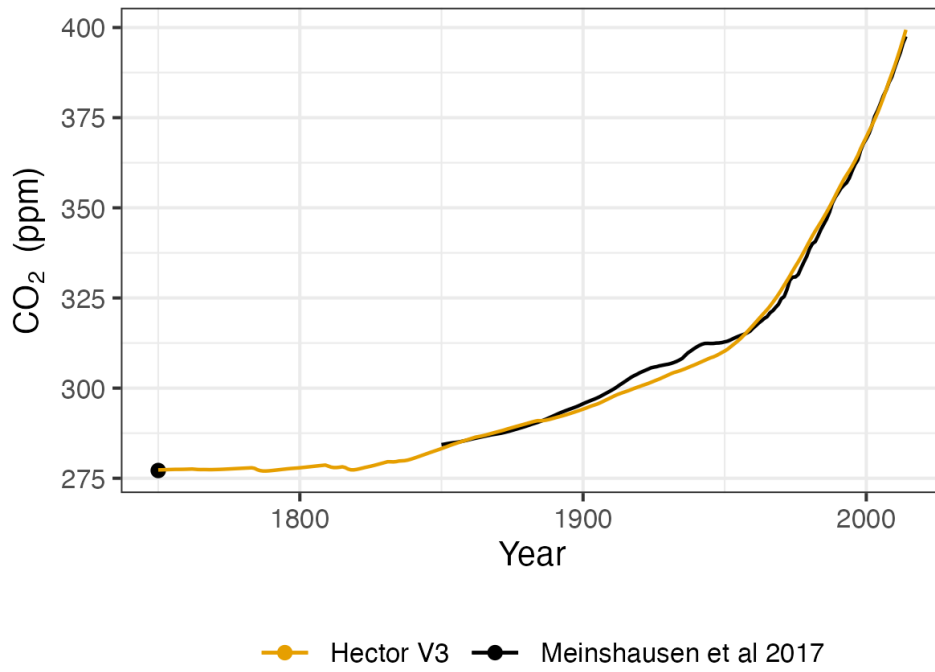


560  
 561  
 562  
 563



Deleted:

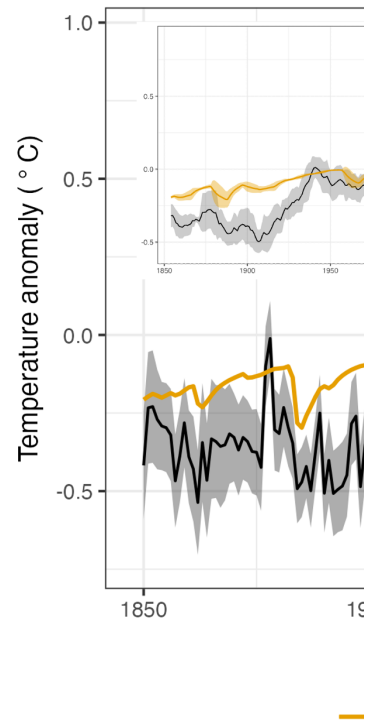
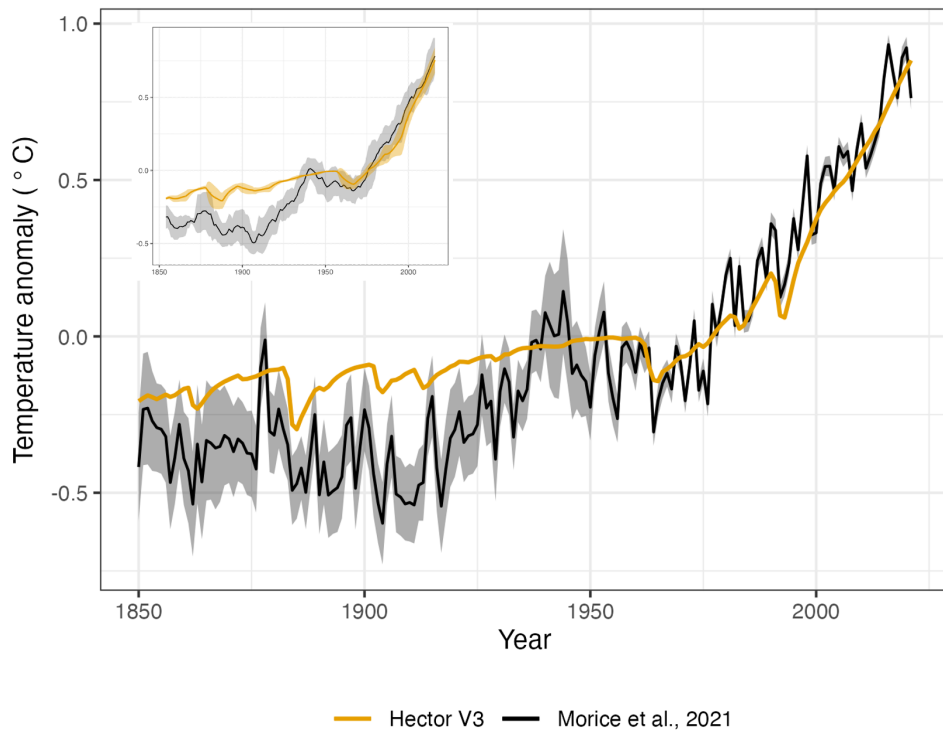
565 **Figure 2. Hector CO<sub>2</sub> concentrations (orange) compared with the CMIP6 (Meinshausen et al., 2017) CO<sub>2</sub>**  
566 **concentrations observational product (black)**



Deleted:

567  
568

570 **Figure 3. Global mean surface temperature anomaly relative to 1951-1980 for Hector (orange) and HadCRUT 5**  
571 **global mean surface temperature observations (Morice et al., 2021) (black, with associated uncertainty). The inset**  
572 **figure shows the rolling decadal average.**

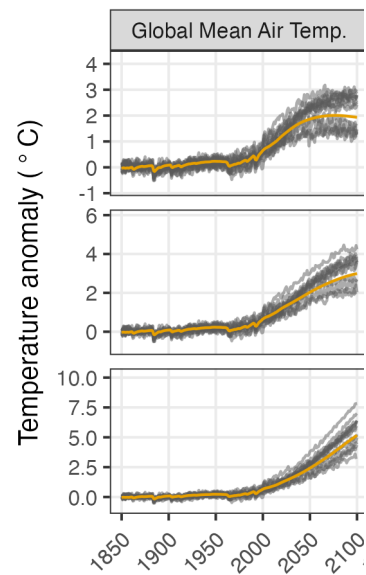
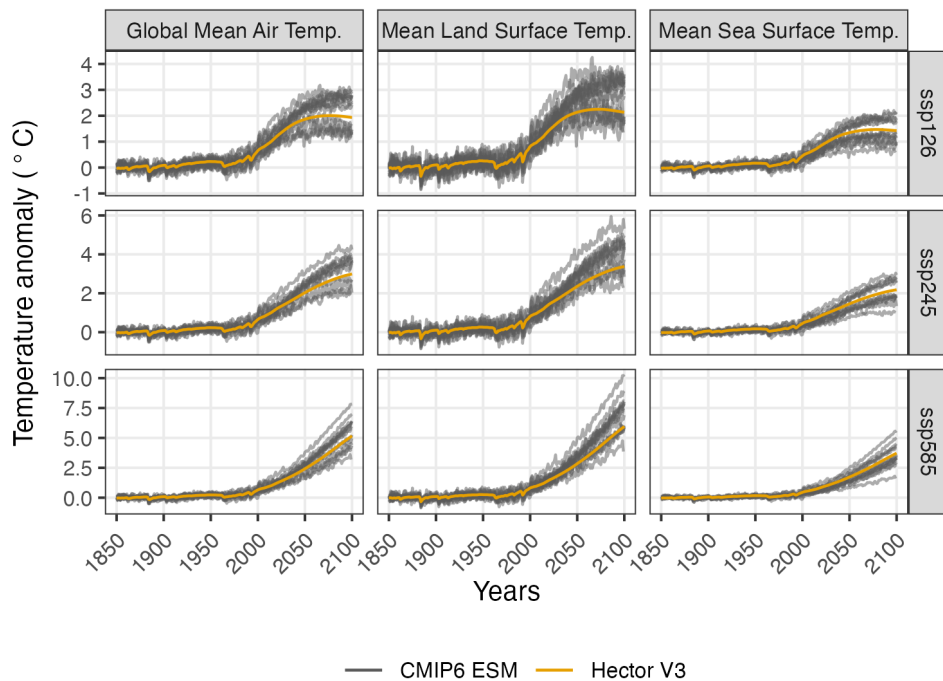


Deleted:

573  
574



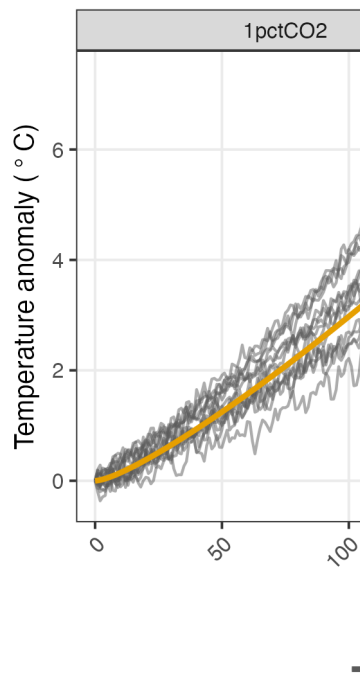
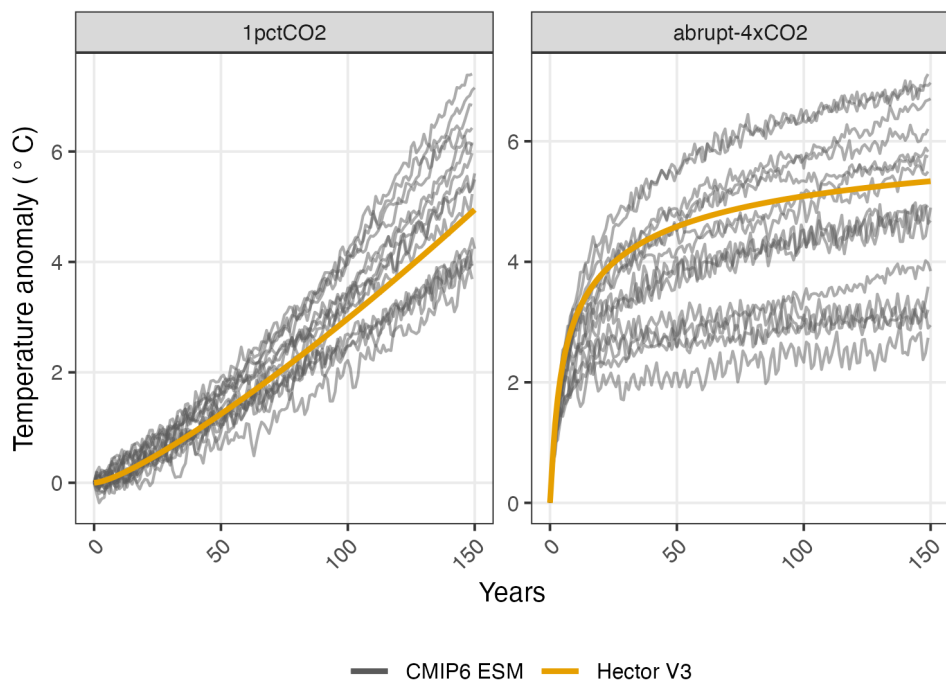
576 **Figure 4. Global, land, and sea surface temperature anomalies relative to 1850-1900 from concentration-driven**  
 577 **(“constrained”) Hector, in orange, and temperature output from 15 different CMIP6-participating ESMs, in grey**  
 578 **(see Supplementary Table 8).**



Deleted:

579  
580

582 **Figure 5. Global temperature anomaly from 1% CO<sub>2</sub> and 4xCO<sub>2</sub> stylized experiments (Eyring et al., 2016) for Hector**  
583 **(orange) and 15 different CMIP6 participating ESMs (grey lines; see Supplementary Table 8).**



Deleted:

584